NANO LETTERS

pubs.acs.org/NanoLett Letter

Observation of Giant Surface Second-Harmonic Generation Coupled to Nematic Orders in the van der Waals Antiferromagnet $FePS_3$

Zhuoliang Ni, Nan Huang, Amanda V. Haglund, David G. Mandrus, and Liang Wu*

Cite This: *Nano Lett.* 2022, 22, 3283−3288 Read Online

ACCESS | Metrics & More | Article Recommendations | Supporting Information

ABSTRACT: Second-harmonic generation has been applied to study lattice, electronic, and magnetic proprieties in atomically thin materials. However, inversion symmetry breaking is usually required for the materials to generate a large signal. In this work, we report a giant second-harmonic generation that arises below the Néel temperature in few-layer centrosymmetric $FePS_3$. A layer-dependent study indicates the detected signal is from the second-order nonlinearity of the surface. The magnetism-induced surface second-harmonic response is 2 orders of magnitude larger than those reported in other magnetic systems, with the surface nonlinear susceptibility reaching 0.08−0.13 nm^2/V in 2−5 L samples. By combing linear dichroism and second-harmonic generation experiments, we further confirm the giant second-harmonic generation is coupled to nematic orders formed by the three possible Zigzag antiferromagnetic domains. Our study shows that the surface second-harmonic generation is also a sensitive tool to study antiferromagnetic states in centrosymmetric atomically thin materials.

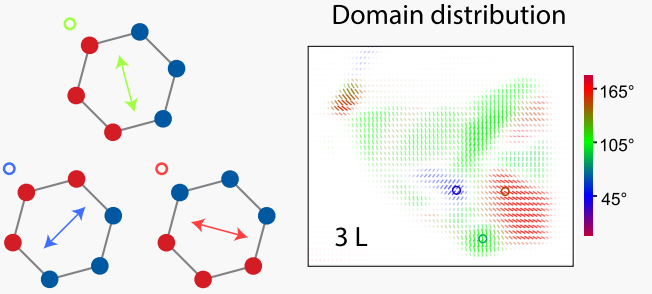

KEYWORDS: *antiferromagnetism, two-dimensional magnets, surface second-harmonic generation, nematic order*

INTRODUCTION

Because of its sensitivity to the symmetry-breaking phases, second-harmonic generation (SHG) has been applied to study many properties in van der Waals materials, including layer numbers,[1,2] crystal orientations,[1−3] ferroelectric orders,[4−6] charge-density waves,[7,8] lattice structure,[9,10] magnetic orders,[11−13] and multiferroic orders.[14,15] The commonly known SHG response is from a nonzero electric-dipole term from the bulk states, which requires the inversion symmetry breaking of the materials. For centrosymmetric materials, the bulk electric-dipole term is prohibited. However, the inversion symmetry is naturally broken on the sample surface, which enables SHG responses from the surface layers.[16,17]

The surface SHG results from the breaking of inversion symmetry at an interface. It was detected in various metal[18−21] and molecular systems,[22,23] but has seldomly been reported in ultrathin van der Waals materials. The bulk electric-dipole contribution is nearly proportional to the sample thickness when the sample thickness is smaller than the coherence length of the SHG light, but the surface term remains nearly independent of the thickness. In principle, a surface SHG signal could be comparable to the bulk SHG signal in ultrathin noncentrosymmetric materials. As a result, surface SHG provides a possible way to detect emergent electronic and magnetic properties without the requirement of inversion symmetry breaking.

The transition metal thiophosphates MPS_3 (M = Mn, Fe, Ni, Co) provide a good platform to study 2D antiferromagnetism with different magnetic anisotropy.[24−27] Here we focus on two compounds $FePS_3$ and $MnPS_3$, with the same lattice structure. Because of the different magnetic anisotropy, $FePS_3$ has Zigzag-type antiferromagnetism where inversion symmetry is preserved[28−30] (Figure 1a), but $MnPS_3$ has Néel-type antiferromagnetism where the inversion symmetry is broken[28,31] (Figure 1b). According to the previous studies, in the Néel-type antiferromagnet $MnPS_3$, an electric-dipole SHG signal induced by the magnetism is observed down to bilayer samples.[12,32] It is usually believed, however, that the second-harmonic response is insensitive to the Zigzag-type antiferromagnetic orders because of the preserved inversion symmetry.[12]

In the monolayer $FePS_3$, the Fe atoms carrying spins form the honeycomb lattice with 3-fold rotational symmetry. The space group without magnetism is $P\bar{3}1m$. In multilayer $FePS_3$, the monoclinic stacking breaks the 3-fold rotational symmetry and the space group without magnetism falls into $2/m$.[17] When the $FePS_3$ is below the Néel temperature (118 K for bulk), a Zigzag-type antiferromagnetic order forms (Figure 1a), according to the neutron scattering measurement.[28−30] The

Received: January 18, 2022
Revised: April 5, 2022
Published: April 12, 2022

https://doi.org/10.1021/acs.nanolett.2c00212
Nano Lett. 2022, 22, 3283−3288

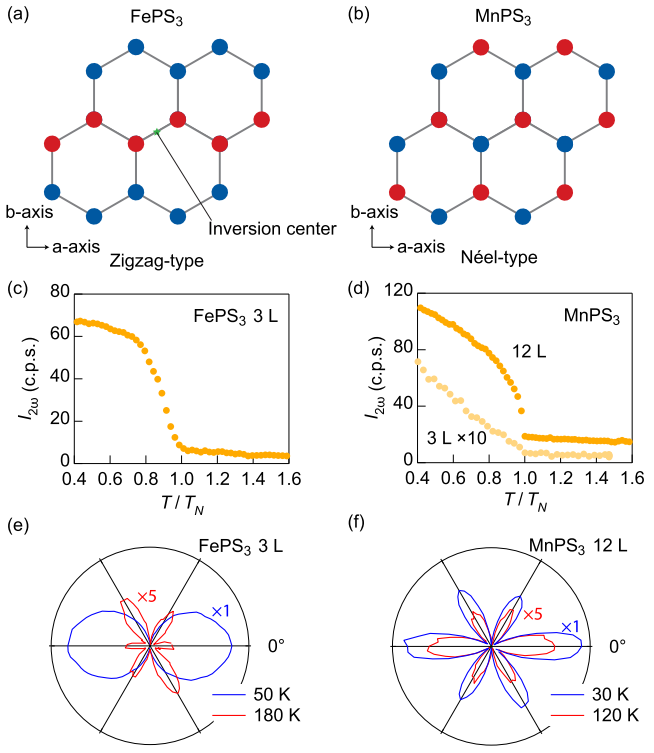

Figure 1. (a, b) Spin structure of $FePS_3$ (Zigzag-type) and $MnPS_3$ (Néel-type) in the monolayer. Red and blue circles represent opposite spin directions on the Fe/Mn atoms. (c, d) Temperature dependence of SHG intensity of $FePS_3$ and $MnPS_3$ samples. (e, f) Polarization-resolved SHG intensity of $FePS_3$ and $MnPS_3$ samples below and above Néel temperature. The polarizations of incident photons and output photons are kept parallel and rotated simultaneously.

magnetism persists to the monolayer according to the Raman spectroscopy.[33,34] Nevertheless, there has been some controversy over the Zigzag directions and domains. Some neutron scattering experiments suggest the Zigzag direction is along the *a*-axis,[28] whereas others suggest the Zigzag direction can be 120° from the *a*-axis.[29] A more recent neutron scattering work reports the coexistence of the three Zigzag directions in a $FePS_3$ crystal, which is argued to be related with the crystal twinning rather than magnetic domains,[30] and also concluded the structure twinning effect in the earlier work of ref 29. A most recent linear dichroism (LD) measurement on a multilayer $FePS_3$ shows the coexisting of two different Zigzag directions on areas with different thickness.[35,36]

In this paper, we show that the centrosymmetric Zigzag orders in $FePS_3$ can produce a surprisingly large surface second-harmonic generation down to the bilayer, which is coupled to the Zigzag antiferromagnetic orders. To investigate the origin of the multidomains, we performed spacial scanning of polarization-dependent SHG and LD measurements simultaneously on a 3 layer (L) sample with a single structure domain and observed three magnetic domains with Zigzag directions 120° to each other. We further showed that the surface SHG also rotated by 120° between these three domains. The surface SHG is coupled to the Zigzag direction, and, therefore, few-layer $FePS_3$ samples form the antiferromagnetic nematic orders without structure twinning.

RESULTS AND DISCUSSION

Figure 1d shows the temperature dependence of the SHG intensity of 3 and 12 L $MnPS_3$ flakes. A sudden rise in SHG intensity below the Néel temperature of 78 K is observed, because the Néel-type antiferromagnetism breaks the inversion symmetry in this system.[12,32] The SHG response is believed to have two parts, including the electric-dipole term and the electric-quadruple term:

$$E_i(2\omega) \propto \int_0^d \chi^D_{ijk} E_j(\omega) E_k(\omega) \mathrm{d}z + \int_0^d \chi^Q_{ijzk} E_j(\omega) k_z E_k(\omega) \mathrm{d}z \quad (1)$$

where χ^D_{ijk}, χ^Q_{ijkl} are the susceptibility tensor of electric-dipole and electric-quadruple terms, respectively. $E_i(\omega)$ is the electric field from the fundamental light, and d is the sample thickness. Note that the SHG signal scales with the effective thickness as reported in the previous research.[32]

The SHG intensity of the 3 L $FePS_3$, to our surprise, is also coupled to the centrosymmetric Zigzag orders, as it shows a phase transition at the Néel temperature of 116 K (Figure 1c). Moreover, the 3 L $FePS_3$ generates only a slightly smaller SHG intensity than the 12 L $MnPS_3$ and 10 times larger than 3 L $MnPS_3$, which is quite surprising considering that the $FePS_3$ sample is centrosymmetric but $MnPS_3$ breaks inversion symmetry. Figure 1e shows the polarization-dependent SHG intensity ($E_\omega \| E_{2\omega}$) of the same $FePS_3$ sample measured above and below the Néel temperature. At 50 K, the SHG pattern has two lobes, which changes dramatically from the 6-lobe shape from the lattice at 180 K. Because the second-order susceptibility is directly coupled to the symmetry of the system, the arising large 2-fold SHG signal in $FePS_3$ indicates that the SHG comes from the magnetism. Different from $FePS_3$, the shapes of the SHG polar patterns of the 12 L Néel-type $MnPS_3$ remain the same above and below Néel temperature, whereas the SHG intensity changes (Figure 1f).

Because of the presence of the inversion symmetry in $FePS_3$, the bulk electric-dipole term is not allowed. The magnetism-coupled SHG change could come from the electric-quadruple term or/and the surface term. To better understand the origin of the large SHG response in $FePS_3$, we studied the thickness dependence. The results of polarization dependence and temperature dependence are shown in Figure 2. We found that from a thick flake to a bilayer, the SHG intensity above the Néel temperature drops dramatically, but the magnetism-coupled signal below T_N remains in the same order of magnitude. The former is easy to understand because the SHG above the Néel temperature is from the electric-quadruple contribution, which scales quadratically on the sample thickness when the sample thickness is less than the coherence length. The latter indicates the magnetism-coupled SHG is insensitive to the thickness, in sharp contrast to $MnPS_3$[32] and $MnPSe_3$[13] with noncentrosymmetric magnetic structures. This feature suggests that the magnetism-coupled SHG response does not originate from the bulk (such as a bulk quadruple term or a bulk magnetic dipole term). Therefore, we believe the large magnetism-coupled signal is dominated by the nonlinear response of the surface layers. The SHG response is then written as

https://doi.org/10.1021/acs.nanolett.2c00212
Nano Lett. 2022, 22, 3283−3288

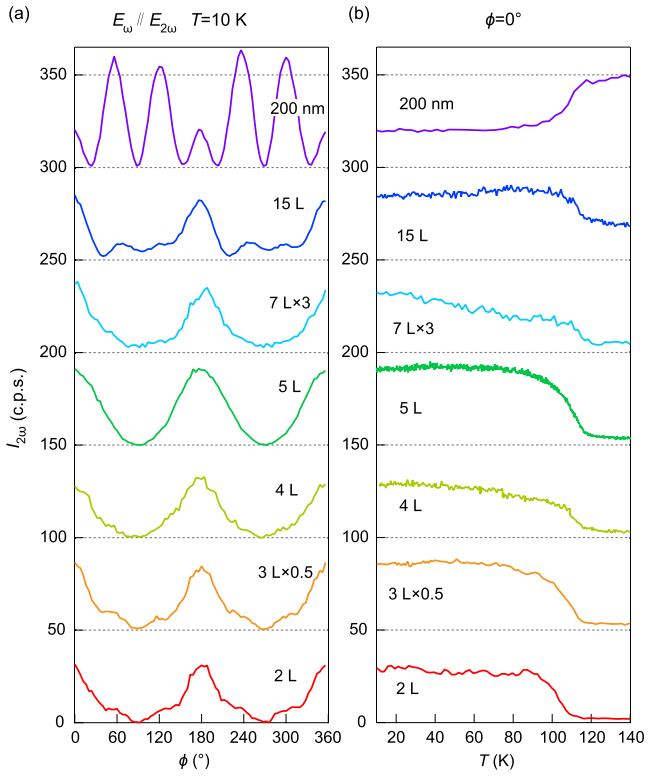

Figure 2. (a) SHG intensity as a function of polarization angle ϕ measured at different sample thickness. The polarizations of incident photons and output photons are kept parallel and rotated simultaneously. (b) Temperature-dependent SHG intensity measured at different sample thicknesses. Both polarizations of incident and output photons are kept at 0°. For both a and b, an offset of 50 c.p.s. is applied between different curves.

$$E_i(2\omega) = \int_0^d \chi^{Q}_{ijzk} E_j(\omega) k_z E_k(\omega) dz + \chi^{s,z}_{ijk} E_j(\omega) E_k(\omega)|_{z=0} \quad (2)$$

where χ^{Q}_{ijkl}, $\chi^{s,z}_{ijk}$ are the susceptibility tensor of bulk electric-quadruple and surface terms, respectively. $E_i(\omega)$ is the electric field from the fundamental light. The magnetism-induced surface SHG is surprisingly large. The ratio of the SHG intensity of a bilayer $FePS_3$ and a bilayer $MnPS_3$ is around 30:1 at 5 K, even though the former is centrosymmetric but the latter breaks the inversion symmetry. By using a GaAs crystal as a reference (see the Supporting Information, Section S2), we show the surface nonlinear susceptibility $|\chi^{s}_{ijk}|$ reaches 0.08–0.13 nm^2/V ($1.9–3.1 \times 10^{-14}$ esu) in 2–5 L samples, which is close to the response from a noncentrosymmetric MoS_2 monolayer,[1] whose inversion symmetry is broken by the lattice. Note that the surface SHG from $FePS_3$ is from the magnetism. When compared to other magnetism-induced surface SHG on previous reported thin-film materials,[20,21,37] the response from $FePS_3$ is at least 2 orders of magnitude larger in terms of the second-order susceptibility $|\chi^{s}_{ijk}|$. Except from the large surface nonlinear optical response, it is interesting to note that $FePS_3$ also has a giant antiferromagnetism-coupled linear optical response.[35,38]

In a monolayer $FePS_3$, the Fe atoms with out-of-plane spins form the honeycomb lattice with 3-fold rotational symmetry. In multilayer $FePS_3$, the monoclinic stacking breaks the 3-fold rotational symmetry very weakly. As the polarization-dependent SHG polar plots show a 6-fold pattern (see the Supporting Information, Section S1, for the high-temperature data in a bulk sample). Also, the negligible polarization-dependent LD at high temperature[35] suggests the system still has an approximately 3-fold rotational symmetry in its electronic structure without magnetism, which gives rise to different

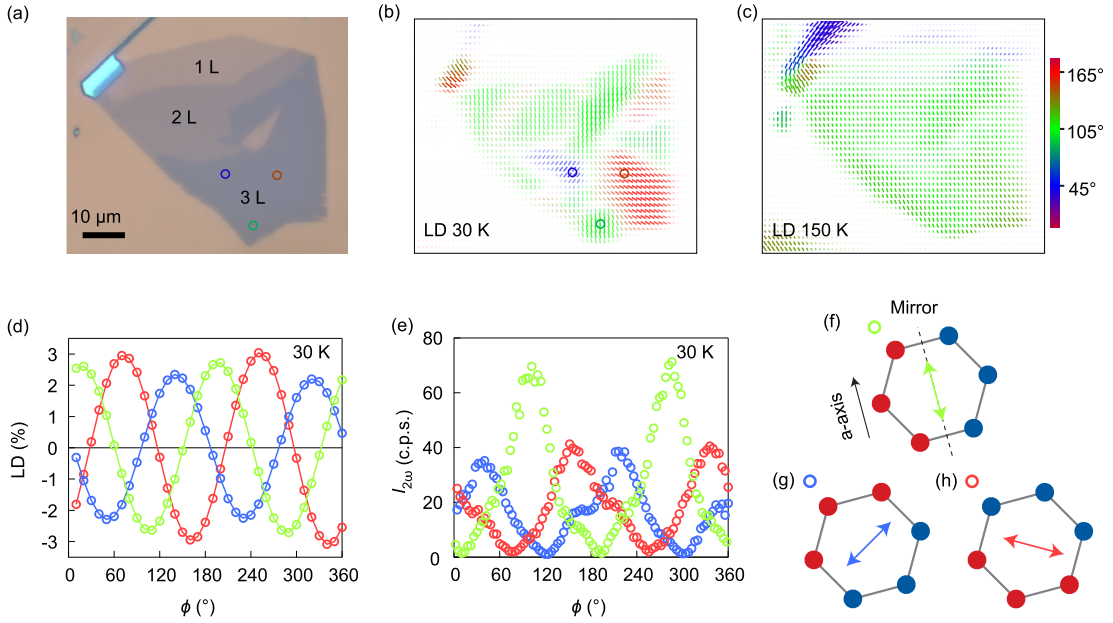

Figure 3. (a) Optical image of a multilayer $FePS_3$ flake, including 1 to 3 L. (b, c) LD mapping of the same area in panel a at 30 and 150 K. The direction of small segments on each point represents the polarization direction when the LD is at the valley. The length of the segments represents the magnitude of the LD. Three colors are used to indicate three nematic domains. (d, e) Polarization-dependent LD and SHG intensity of the three points chosen from three domains marked by open circles on panel b. (f–h) Schematic diagrams showing three possible nematic domains formed by Zigzag antiferromagnetic orders. Red and blue circles indicate opposite spin directions on Fe atoms. Only the configuration in panel f preserves the mirror symmetry of the whole system.

https://doi.org/10.1021/acs.nanolett.2c00212
Nano Lett. 2022, 22, 3283–3288

Zigzag-order states with very close energy. The Zigzag order, on the other hand, strongly picks up a direction that breaks the approximate 3-fold rotational symmetry, resulting in anisotropic linear and nonlinear optical properties that are 120° to each other (see Figure 3 and discussions below).

To address the origin of the multidomains, we perform the LD and SHG measurements on a large 3 L $FePS_3$ sample, as thick samples often have stacking faults (see the Supporting Information, Section S3). Figure 3a is the optical image of the sample, and Figure 3b is the LD mapping at 30 K in the same region. The direction and the length of each segment at each point represent the valley location in the angle dependence and the magnitude of the LD, respectively. Three colors are used to emphasize three Zigzag directions with an interval of 120°. Three points in the green, blue, and red regions of the 3 L sample in Figure 3d are chosen to show the polarization-dependent LD, which indicates the coexistence of three Zigzag directions. Note that a homogeneous LD direction distribution is observed at 150 K (Figure 3c), excluding the influence of the stacking fault. The polarization-dependent SHG measurement at the same three points (Figure 3e) also shows the SHG polar patterns are also rotated by 120° and follow the Zigzag directions. We also combine the LD and SHG measurements to show that the valley position of the LD and the peak position of the SHG indicate the Zigzag direction (see the Supporting Information, Section S1). It is interesting to note the intensity of the green curve is larger than the other two, and the green curve has a mirror symmetry but the red and blue ones do not. According to the LD measurement at 150 K, the Zigzag direction of the green region is along the *a*-axis, which preserves the mirror symmetry of the system (Figure 3f), whereas the Zigzag orders of the blue (Figure 3g) and red (Figure 3h) region break the mirror symmetry because the Zigzag direction is different from the layer-stacking direction.

From the experimental data, it is not clear what causes different Zigzag order distribution in the $FePS_3$ samples. Note the LD mapping does not change after a thermal cycle (see the Supporting Information, Section S4). On the basis of the similar behavior of other materials, we believe strain is likely responsible for the Zigzag order distribution, as the 3-fold rotational symmetry is only very weakly broken above T_N. A strain-tuning measurement as the previous study[13] by a polymer substrate is not possible because of the large and randomly distributed LD signal from the uneven polymer substrate. Similarly, the polymer substrate generates a strong photoluminescence signal that overwhelms the SHG signal of the samples. Further experiments, for instance, adding strain directly on the wafer, are called for to understand the nematic orders of the materials.

To summarize, we discovered a giant surface SHG signal on $FePS_3$ samples coupled to the centrosymmetric Zigzag-type antiferromagnetic orders. The surface nonlinear susceptibility $|\chi^s_{ijk}|$ reaches 0.08−0.13 nm^2/V ($1.9-3.1 \times 10^{-14}$ esu) in 2−5 L samples. The direction of the Zigzag order is resolved by polarization-dependent SHG and LD measurements. Nematic states with three Zigzag directions coexist in a single crystal, which points to a new mechanism other than the structure twinning. The observed giant surface SHG signal coupled to the centrosymmetric antiferromagnetic orders suggests that SHG is a good probe for emergent states in atomically thin materials even without inversion symmetry breaking.

METHODS

Sample Preparation. To perform optical measurements in the cryostat, we mounted the bulk $FePS_3$ on copper by a thin layer of GE varnish. The few-layer samples were directly exfoliated on the SiO_2/Si wafer in air and then transferred into the vacuum chamber of a cryostat. In our experiment, we did not see noticeable degradation of the few-layer $FePS_3$ in air. However, we still controlled the exposure time to be less than 20 min.

Second-Harmonic Generation Measurement. In the SHG experiment, we used an 800 nm Ti-sapphire laser (80 MHz, ∼50 fs) as the fundamental light. The beam is focused by a 50× objective to the beam spot size of around 2 μm. A typical laser power of 400 μW is applied. No noticeable sample degradation was observed under the laser exposure and thermal cycles. The same objective was used to collect the reflected 400 nm beam, which is then detected by a photon counter. A half-wave plate and a linear polarizer were used to control the polarization of the incident and outgoing beams, respectively. The coherence length of the reflected SHG can be calculated by $\frac{\lambda}{4\pi(\tilde{n}_\omega + \tilde{n}_{2\omega})}$, which is the effective thickness of the sample that can generate the in-phase reflected second-harmonic photons.

Linear Dichroism Measurement. The polarization-dependent LD was measured by taking the reflection difference between two axes that are perpendicular to each other: $\eta(\phi) = \frac{I_R(\phi) - I_R(\phi + 90°)}{I_R(\phi) + I_R(\phi + 90°)}$ under the same 800 nm Ti-sapphire laser as the SHG measurement. A photoelastic modulator was used to modulate the polarization at 42 kHz. A half-wave plate was placed right before the objective to control the polarization of the incident light.

ASSOCIATED CONTENT

Supporting Information

The Supporting Information is available free of charge at https://pubs.acs.org/doi/10.1021/acs.nanolett.2c00212.

Symmetry analysis of the surface SHG of $FePS_3$; estimation of the surface nonlinear susceptibility χ^s_{ijk} of the few-layer $FePS_3$; Zigzag domains measured in a $FePS_3$ thick flake; discussion on the enhancement of the magnetism-coupled SHG response in thin samples; more data on linear dichroism mapping of the 3 L $FePS_3$ sample; linear and nonlinear responses of the monolayer $FePS_3$ (PDF)

AUTHOR INFORMATION

Corresponding Author

Liang Wu − *Department of Physics and Astronomy, University of Pennsylvania, Philadelphia, Pennsylvania 19104, United States*; Email: liangwu@sas.upenn.edu

Authors

Zhuoliang Ni − *Department of Physics and Astronomy, University of Pennsylvania, Philadelphia, Pennsylvania 19104, United States*; orcid.org/0000-0002-3135-4018

Nan Huang − *Department of Materials Science and Engineering, University of Tennessee, Knoxville, Tennessee 37996, United States*

Amanda V. Haglund − *Department of Materials Science and Engineering, University of Tennessee, Knoxville, Tennessee 37996, United States*

https://doi.org/10.1021/acs.nanolett.2c00212
Nano Lett. 2022, 22, 3283−3288

David G. Mandrus − *Department of Materials Science and Engineering, University of Tennessee, Knoxville, Tennessee 37996, United States; Materials Science and Technology Division, Oak Ridge National Laboratory, Oak Ridge, Tennessee 37831, United States;* orcid.org/0000-0003-3616-7104

Complete contact information is available at: https://pubs.acs.org/10.1021/acs.nanolett.2c00212

Notes

The authors declare no competing financial interest.

■ ACKNOWLEDGMENTS

We thank J. Kikkawa, S. Parra, and H. Zhang for help on the experiments, and O. Tchernyshyov for helpful discussions. The project design, data collection, and analysis were supported by L.W.'s startup package at the University of Pennsylvania. The development of the SHG photon counter was supported by the ARO under Grant W911NF1910342. The development of the scanning imaging microscope was partially supported by the ARO under Grants W911NF2110131 and W911NF2020166 and the University Research Foundation. Z.N. is partially supported by the National Science Foundation through the University of Pennsylvania Materials Research Science and Engineering Center (MRSEC) (DMR-1720530). This work was carried out in part at the Singh Center for Nanotechnology, which is supported by the NSF National Nanotechnology Coordinated Infrastructure Program under Grant NNCI-1542153. D.G.M acknowledges support from the Gordon and Betty Moore Foundation's EPiQS Initiative, Grant GBMF9069. Z.N. also acknowledges support from a Vagelos Institute of Energy Science and Technology graduate fellowship at the University of Pennsylvania.

■ REFERENCES

(1) Li, Y.; Rao, Y.; Mak, K. F.; You, Y.; Wang, S.; Dean, C. R.; Heinz, T. F. Probing symmetry properties of few-layer MoS_2 and h-BN by optical second-harmonic generation. *Nano Lett.* **2013**, *13*, 3329−3333.

(2) Malard, L. M.; Alencar, T. V.; Barboza, A. P. M.; Mak, K. F.; de Paula, A. M. Observation of intense second harmonic generation from MoS_2 atomic crystals. *Phys. Rev. B* **2013**, *87*, 201401.

(3) Kumar, N.; Najmaei, S.; Cui, Q.; Ceballos, F.; Ajayan, P. M.; Lou, J.; Zhao, H. Second harmonic microscopy of monolayer MoS_2. *Phys. Rev. B* **2013**, *87*, 161403.

(4) Liu, F.; You, L.; Seyler, K. L.; Li, X.; Yu, P.; Lin, J.; Wang, X.; Zhou, J.; Wang, H.; He, H.; et al. Room-temperature ferroelectricity in $CuInP_2S_6$ ultrathin flakes. *Nat. Communs.* **2016**, *7*, 12357.

(5) Xiao, J.; Zhu, H.; Wang, Y.; Feng, W.; Hu, Y.; Dasgupta, A.; Han, Y.; Wang, Y.; Muller, D. A.; Martin, L. W.; Hu, P.; Zhang, X. Intrinsic two-dimensional ferroelectricity with dipole locking. *Phys. Rev. Lett.* **2018**, *120*, 227601.

(6) Xue, F.; Hu, W.; Lee, K.-C.; Lu, L.-S.; Zhang, J.; Tang, H.-L.; Han, A.; Hsu, W.-T.; Tu, S.; Chang, W.-H.; Lien, C.-H.; He, J.-H.; Zhang, Z.; Li, L.-J.; Zhang, X. Room-temperature ferroelectricity in hexagonally layered α-In_2Se_3 nanoflakes down to the monolayer limit. *Adv. Funct. Mater.* **2018**, *28*, 1803738.

(7) Fichera, B. T.; Kogar, A.; Ye, L.; Gökce, B.; Zong, A.; Checkelsky, J. G.; Gedik, N. Second harmonic generation as a probe of broken mirror symmetry. *Phys. Rev. B* **2020**, *101*, 241106.

(8) Luo, X.; Obeysekera, D.; Won, C.; Sung, S. H.; Schnitzer, N.; Hovden, R.; Cheong, S.-W.; Yang, J.; Sun, K.; Zhao, L. Ultrafast Modulations and Detection of a Ferro-Rotational Charge Density Wave Using Time-Resolved Electric Quadrupole Second Harmonic Generation. *Phys. Rev. Lett.* **2021**, *127*, 126401.

(9) Zhao, M.; Ye, Z.; Suzuki, R.; Ye, Y.; Zhu, H.; Xiao, J.; Wang, Y.; Iwasa, Y.; Zhang, X. Atomically Phase-Matched Second-Harmonic Generation in a 2D Crystal. *Light Sci. Appl.* **2016**, *5*, e16131.

(10) Wang, Y.; Xiao, J.; Zhu, H.; Li, Y.; Alsaid, Y.; Fong, K. Y.; Zhou, Y.; Wang, S.; Shi, W.; Wang, Y.; et al. Structural phase transition in monolayer $MoTe_2$ driven by electrostatic doping. *Nature* **2017**, *550*, 487−491.

(11) Sun, Z.; et al. Giant nonreciprocal second-harmonic generation from antiferromagnetic bilayer CrI_3. *Nature* **2019**, *572*, 497−501.

(12) Chu, H.; Roh, C. J.; Island, J. O.; Li, C.; Lee, S.; Chen, J.; Park, J.-G.; Young, A. F.; Lee, J. S.; Hsieh, D. Linear magnetoelectric phase in ultrathin $MnPS_3$ probed by optical second harmonic generation. *Phys. Rev. Lett.* **2020**, *124*, 027601.

(13) Ni, Z.; Haglund, A.; Wang, H.; Xu, B.; Bernhard, C.; Mandrus, D.; Qian, X.; Mele, E.; Kane, C.; Wu, L. Imaging the Néel vector switching in the monolayer antiferromagnet $MnPSe_3$ with strain-controlled Ising order. *Nat. Nanotechnol.* **2021**, *16*, 782−787.

(14) Song, Q.; Occhialini, C. A.; Ergeçen, E.; Ilyas, B.; Amoroso, D.; Barone, P.; Kapeghian, J.; Watanabe, K.; Taniguchi, T.; Botana, A. S.; et al. Experimental realization of a single-layer multiferroic. *Nature* **2022**, *602*, 601−605.

(15) Ju, H.; Lee, Y.; Kim, K.-T.; Choi, I. H.; Roh, C. J.; Son, S.; Park, P.; Kim, J. H.; Jung, T. S.; Kim, J. H.; et al. Possible persistence of multiferroic order down to bilayer limit of van der Waals material NiI_2. *Nano Lett.* **2021**, *21*, 5126−5132.

(16) Bloembergen, N.; Pershan, P. S. Light Waves at the Boundary of Nonlinear Media. *Phys. Rev.* **1962**, *128*, 606−622.

(17) Guyot-Sionnest, P.; Chen, W.; Shen, Y. R. General considerations on optical second-harmonic generation from surfaces and interfaces. *Phys. Rev. B* **1986**, *33*, 8254−8263.

(18) Bloembergen, N.; Chang, R. K.; Lee, C. H. Second-Harmonic Generation of Light in Reflection from Media with Inversion Symmetry. *Phys. Rev. Lett.* **1966**, *16*, 986−989.

(19) Lee, C. H.; Chang, R. K.; Bloembergen, N. Nonlinear Electroreflectance in Silicon and Silver. *Phys. Rev. Lett.* **1967**, *18*, 167−170.

(20) Reif, J.; Zink, J. C.; Schneider, C.-M.; Kirschner, J. Effects of surface magnetism on optical second harmonic generation. *Phys. Rev. Lett.* **1991**, *67*, 2878−2881.

(21) Reif, J.; Rau, C.; Matthias, E. Influence of magnetism on second harmonic generation. *Phys. Rev. Lett.* **1993**, *71*, 1931−1934.

(22) Chen, C. K.; Heinz, T. F.; Ricard, D.; Shen, Y. R. Detection of molecular monolayers by optical second-harmonic generation. *Phys. Rev. Lett.* **1981**, *46*, 1010−1012.

(23) Heinz, T. F.; Chen, C. K.; Ricard, D.; Shen, Y. R. Spectroscopy of Molecular Monolayers by Resonant Second-Harmonic Generation. *Phys. Rev. Lett.* **1982**, *48*, 478−481.

(24) Joy, P. A.; Vasudevan, S. Magnetism in the layered transition-metal thiophosphates MPS_3 (M = Mn, Fe, and Ni). *Phys. Rev. B* **1992**, *46*, 5425−5433.

(25) Li, X.; Cao, T.; Niu, Q.; Shi, J.; Feng, J. Coupling the valley degree of freedom to antiferromagnetic order. *Proc. Natl. Acad. Sci. U. S. A.* **2013**, *110*, 3738−3742.

(26) Sivadas, N.; Daniels, M. W.; Swendsen, R. H.; Okamoto, S.; Xiao, D. Magnetic ground state of semiconducting transition-metal trichalcogenide monolayers. *Phys. Rev. B* **2015**, *91*, 235425.

(27) Chittari, B. L.; Park, Y.; Lee, D.; Han, M.; MacDonald, A. H.; Hwang, E.; Jung, J. Electronic and magnetic properties of single-layer MPX_3 metal phosphorous trichalcogenides. *Phys. Rev. B* **2016**, *94*, 184428.

(28) Kurosawa, K.; Saito, S.; Yamaguchi, Y. Neutron Diffraction Study on $MnPS_3$ and $FePS_3$. *J. Phys. Soc. Jpn.* **1983**, *52*, 3919−3926.

(29) Rule, K. C.; McIntyre, G. J.; Kennedy, S. J.; Hicks, T. J. Single-crystal and powder neutron diffraction experiments on $FePS_3$: Search for the magnetic structure. *Phys. Rev. B* **2007**, *76*, 134402.

(30) Lancon, D.; Walker, H. C.; Ressouche, E.; Ouladdiaf, B.; Rule, K. C.; McIntyre, G. J.; Hicks, T. J.; Rønnow, H. M.; Wildes, A. R. Magnetic structure and magnon dynamics of the quasi-two-dimensional antiferromagnet $FePS_3$. *Phys. Rev. B* **2016**, *94*, 214407.

(31) Ressouche, E.; Loire, M.; Simonet, V.; Ballou, R.; Stunault, A.; Wildes, A. Magnetoelectric $MnPS_3$ as a candidate for ferrotoroidicity. *Phys. Rev. B* **2010**, *82*, 100408.
(32) Ni, Z.; Zhang, H.; Hopper, D. A.; Haglund, A. V.; Huang, N.; Jariwala, D.; Bassett, L. C.; Mandrus, D. G.; Mele, E. J.; Kane, C. L.; Wu, L. Direct Imaging of Antiferromagnetic Domains and Anomalous Layer-Dependent Mirror Symmetry Breaking in Atomically Thin $MnPS_3$. *Phys. Rev. Lett.* **2021**, *127*, 187201.
(33) Lee, J.-U.; Lee, S.; Ryoo, J. H.; Kang, S.; Kim, T. Y.; Kim, P.; Park, C.-H.; Park, J.-G.; Cheong, H. Ising-type magnetic ordering in atomically thin $FePS_3$. *Nano Lett.* **2016**, *16*, 7433−7438.
(34) Wang, X.; Du, K.; Fredrik Liu, Y. Y.; Hu, P.; Zhang, J.; Zhang, Q.; Owen, M. H. S.; Lu, X.; Gan, C. K.; Sengupta, P.; et al. Raman spectroscopy of atomically thin two-dimensional magnetic iron phosphorus trisulfide ($FePS_3$) crystals. *2D Mater.* **2016**, *3*, 031009.
(35) Zhang, Q.; Hwangbo, K.; Wang, C.; Jiang, Q.; Chu, J.-H.; Wen, H.; Xiao, D.; Xu, X. Observation of giant optical linear dichroism in a zigzag antiferromagnet $FePS_3$. *Nano Lett.* **2021**, *21*, 6938−6945.
(36) Zhang, X.-X.; Jiang, S.; Lee, J.; Lee, C.; Mak, K. F.; Shan, J. Spin dynamics slowdown near the antiferromagnetic critical point in atomically thin $FePS_3$. *Nano Lett.* **2021**, *21*, 5045−5052.
(37) Pan, R.-P.; Wei, H. D.; Shen, Y. R. Optical second-harmonic generation from magnetized surfaces. *Phys. Rev. B* **1989**, *39*, 1229−1234.
(38) Zhang, H.; Ni, Z.; Stevens, C. E.; Bai, A.; Peiris, F.; Hendrickson, J. R.; Wu, L.; Jariwala, D. Cavity-enhanced linear dichroism in a van der Waals antiferromagnet. *Nat. Photonics* **2022**, *16*, 311−317.

https://doi.org/10.1021/acs.nanolett.2c00212
Nano Lett. 2022, 22, 3283−3288